Noise analysis and optical response of microwave kinetic inductance detectors with an optical stack

Paul Nicaise, Jie Hu, Christine Chaumont, Piercarlo Bonifacio, Michel Piat, Hervé Geoffray, Faouzi Boussaha

Noise Analysis and Optical Response of Microwave Kinetic Inductance Detectors with an Optical Stack

Paul Nicaise[1]‡, Jie Hu[1], Christine Chaumont[1], Piercarlo Bonifacio[2], Michel Piat[3], Hervé Geoffray[4] and Faouzi Boussaha[1]

[1]GEPI, Observatoire de Paris, Université PSL, CNRS, 75014 Paris, France
[2]GEPI, Observatoire de Paris, Université PSL, CNRS, 92195 Meudon, France
[3]Université de Paris, CNRS, Astroparticule et Cosmologie, 75013 Paris, France
[4]French Space Agency CNES, 31400 Toulouse, France

E-mail: nicaise@chalmers.se

Abstract. We report on the experimental investigation of optical coupling for superconducting microresonators known as Microwave Kinetic Inductance Detectors (MKIDs) in the visible and near-infrared bands. MKIDs are photon-counting, time and energy-resolving detectors that still suffer from a poor quantum efficiency. To improve this efficiency, we propose to add a superconducting reflective layer below the absorbing part of the detector separated by a transparent Al_2O_3 layer with a quarter-wavelength thickness optimized around a single wavelength $\lambda = 405$ nm. We have first fabricated samples patterned from stoichiometric TiN ($T_c \sim 4$ K), one with the full optical stack, one without for reference and one with a partial optical stack in order to characterize the noise influence of each layer individually. We observe that the full optical stack geometry has the most impact on the resonator's noise and quality factors. A second design was fabricated to characterize the optical response to short pulses of the optical stack and we show from both the frequential noise and optical response that a strong signature of TLS is still present in the optical stack sample. We have finally obtained single-photon response with the optical stack using a more sensitive tri-layer TiN/Ti/TiN absorber ($T_c \sim 1.3$ K) for which a maximum energy resolving power of $R = E/\Delta E \sim 1.3$ was achieved using 405 nm laser pulses at 225 mK. The quality factors of both the reference and optical stack samples are similar but the frequency noise is still a tenfold higher for the optical stack sample which degrades the energy-resolving power of the detector.

‡ Author to whom any correspondence should be addressed.

1. Introduction

Over the past decade, the study of Microwave Kinetic Inductance Detectors (MKIDs) in the visible and Near-Infrared (NIR) bands has been growing exponentially to benefit from their single-photon counting, intrinsic energy resolution, and scalability required in astronomy today [1, 2, 3, 4]. MKIDs are patterned from a single thin-film into LC resonators coupled to a feedline that can simultaneously excite and read out thousands of pixels. When the thin-film has transitioned to the superconducting state below its critical temperature T_c, electrons in the inductor will form Cooper pairs that are accelerated with no dissipation and gain inertia, which translates into kinetic inductance. In the visible to NIR bands, a single photon can down-convert enough Cooper pairs to be detected. The change in quasiparticle density briefly affects the total kinetic inductance. It can be probed through the resonator phase shift, from which we can determine both the photon arrival time and energy. However, most superconducting materials used for optical to NIR MKIDs such as TiN, Al, or PtSi have less than 50% absorbance in the considered operating bands [5].

Several groups have put considerable efforts towards optical coupling in MKIDs in recent years by placing an anti-reflection coating above the absorber and/or a backshot cavity below. However, they have only reported on simulated and experimental spectrometry measurements of unpatterned thin-films, claiming to obtain unity absorption around a single wavelength of 1550 nm using a 20 nm-thick TiN/Ti/TiN multi-layer [6] or near-unity absorption on a wide 500-800 nm band using a 60 nm-thick TiN single-layer [7], with no follow-up on actual MKID devices with such optimizations (i.e. no photon detection performance). To our knowledge, only Mai et al. [8] have fabricated and characterized a 10 nm-thick Al single-layer patterned as an MKID absorber embedded in an optical stack. Unfortunately, they have obtained very low internal quality factors likely due to the additional noise originating from the optical stack.

We have presented the simulation results for our optical stack MKID design in a previous paper and preliminary characterization of the fabricated sample with no clear conclusion due to the low internal quality factors [9]. In this paper, we elaborate on the characterization of samples with two updated designs numbered 1 and 2. As listed in Table 1, we have fabricated and measured three samples using the first design to quantify the noise level of each thin-film constituting the optical stack independently. The first sample is a reference sample with no optical stack, the second one has a dielectric layer below the absorber and the third has the full optical stack. For every sample of the first design, the absorber is made from a single stoichiometric TiN layer ($T_c \approx 4$ K).

The second optical stack design has a capacitor made from Nb. Two different materials for the absorber have been tested, the first being a single stoichiometric TiN layer like for design 1 which has higher quality factors but did not allow for single-photon response. The second material used is a lower-T_c, more sensitive material made from a tri-layer of TiN/Ti/TiN for which we obtained single-photon response and were able to unambiguously compare the energy-resolving power of the optical stack with the tri-layer TiN/Ti/TiN reference sample.

2. Optimization of the optical stack

Fig. 1a shows the sketches of the two different designs discussed in this study. In design 1, the whole lumped-element LC resonator is made from stoichiometric TiN MKIDs like in our previous paper[9] but with a few minor changes shown on the left side of Fig. 1a.

We have reduced the Interdigitated Capacitor (IDC) size from 400×400 to 275×200 µm^2 to get closer to the realistic size of pixels used in full-scale MKID arrays [3, 10, 11] while still being large enough to minimize noise as well as the frequency shift caused by the optical stack parasitic capacitance previously highlighted [9]. As for the meander, its volume is inversely proportional to the MKID sensitivity [12]. However, the surface area of the absorber is limited by the minimum realistic distance we can set a microlens array over the MKIDs array. The only remaining degree of freedom is thus the thickness of the absorber that we have reduced from 60 to 30 nm. This change will naturally decrease the absorption of incident photons but is expected to be largely counterbalanced by the reflector and the increased sensitivity from the smaller meander volume.

We have replaced the gold reflecting layer with Al because of its much higher reflectance between 400 and 600 nm, which is preferable when covering the large 400-1600 nm band of most visible to near-infrared cameras. However, Al has a lower T_c compared to TiN, meaning it still has a large quasiparticle density at the MKID operating temperature $T_c/10 \approx 400$ mK, which might deteriorate the resonator's quality factors. To address this issue, we have placed a higher-T_c Nb layer below the reflector like in the previous design that acts as a proximitizing layer. This means that the superconducting properties of Nb are carried out to the Al layer by the proximity effect. The reflector is separated by a transparent Al_2O_3 dielectric layer with an actual refractive index $n \approx 1.7$. Ideally, the optical stack should consist of multiple dielectric layers

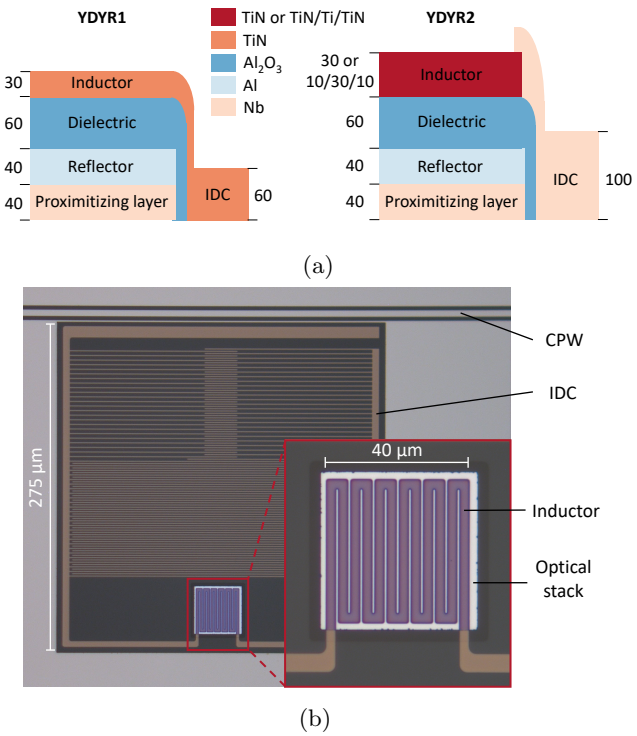

Figure 1: (a) Side-view representation of the first design YDYR1 where the LC resonator is patterned with a single 30 nm-thick TiN thin-film and the second design YDYR2 where the capacitor is Nb and the inductor is either a 30 nm-thick TiN layer or a trilayer TiN/Ti/TiN with thicknesses 10 nm/30 nm/10 nm. The length of the IDCs has been shortened for clarity purposes (all thicknesses are in nanometers). (b) Micrograph of a fabricated MKID resonator and a close-up on the inductor resting on the optical stack.

of different refractive indices and thicknesses to ensure maximum photon coupling to the absorber for every wavelength in the broadband visible to NIR range. However, for demonstration purposes, we will focus on optimizing photon coupling at a single wavelength $\lambda =$ 405 nm, corresponding to the laser diode wavelength available in our characterization setup. In this work, we have used 280 µm-thick c-plane sapphire substrates for all samples. Single-crystal sapphire is known for its negligible dielectric loss tangent $\sim 10^{-6}$ and received a drastic cleaning process before thin-film deposition. Apart from Al_2O_3, all thin-films are sputtered at a pressure $\sim 7 \times 10^{-8}$ mbar on the substrate that receives an RF cleaning beforehand. The features are patterned by photolithography before sputtering and lifted-off afterward. As for Al_2O_3, it is grown by Atomic Layer Deposition (ALD) and subsequently patterned by photolithography and wet etching. ALD helps minimize dielectric tangent loss and allows precise control over the film's thickness, which will be determined for optimal photon coupling at 405 nm.

There are three different samples in design 1: a reference sample on which the resonators are directly deposited onto the substrate with no optical stack (referred to as *No Dielectric No Reflector 1, NDNR1*). A second sample with the dielectric spacer layer below the inductor (*Yes Dielectric No Reflector 1, YDNR1*) which is critical for this study. It will allow to independently quantify the potential loss source coming from the amorphous dielectric layer and the two interfaces between the substrate and the superconductor where native oxide layers usually form. Finally, a third sample has been fabricated with the full optical stack (*Yes Dielectric Yes Reflector 1, YDYR1*), shown on the left side of Fig. 1a, to determine the noise introduced by the parasitic capacitor and the possible optical response improvement.

In the second optical stack design shown on the right side of Fig. 1a, the arms are made of Nb with a higher Cooper pair binding energy, so that photon events are almost exclusively localized in the absorber where the optical stack lies. Since the capacitive arms of the IDC extending to the meander act as unwanted inductive elements, a non-negligible Cooper pair population flows through them. In our current configuration, we illuminate the whole wafer directly so absorption and detection can happen anywhere in these inductive arms. This decoupling also prevents electrical shorts during deposition from the steep optical stack profile between the meander and connecting arms that reaches a thickness of 140 nm in our case. This method does not require an additional lithography and deposition step as it can be patterned simultaneously with the CPW and ground planes. As explained previously, we will present separatly two different materials for the absorber of this second optical stack design: a single stoichiometric TiN layer labeled YDYR2 and a tri-layer of TiN/Ti/TiN labeled YDYR2 tri-layer. We have also fabricated a reference sample for each of these configurations that we labeled respectively NDNR2 and NDNR2 tri-layer.

The incident light arriving on the optical stack can be described as an electromagnetic wave with a complex wave number $\tilde{k}$ and impedance η. The optical stack can be approached as a series of $P = 3$ transmission lines where η_p and $\tilde{k}_p$ are the optical parameters of each line p experimentally measured by ellipsometry. The transfer matrix M_p of line p is cascaded with the other matrices to extract the total optical stack parameters [13]. The whole transfer matrix M_{tot} of the cascaded P layers constituting the optical stack can be expressed as the product of the matrices M_p of each line p by:

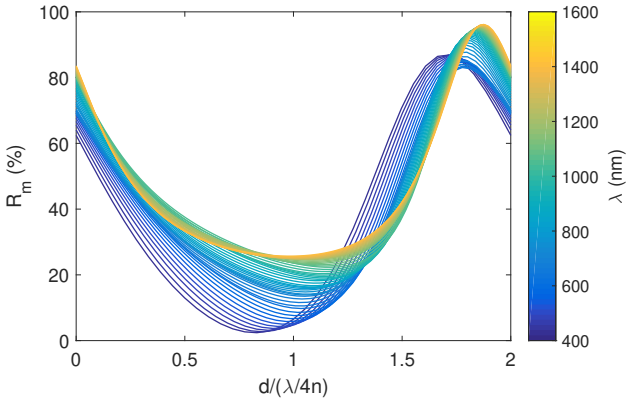

Figure 2: Modelled reflectance off the optical stack (TiN 30 nm, Al_2O_3 variable thickness d and Al 40 nm). d is normalized by the guided quarter-wavelength $\lambda/4n$ with n the Al_2O_3 refractive index at the corresponding wavelength.

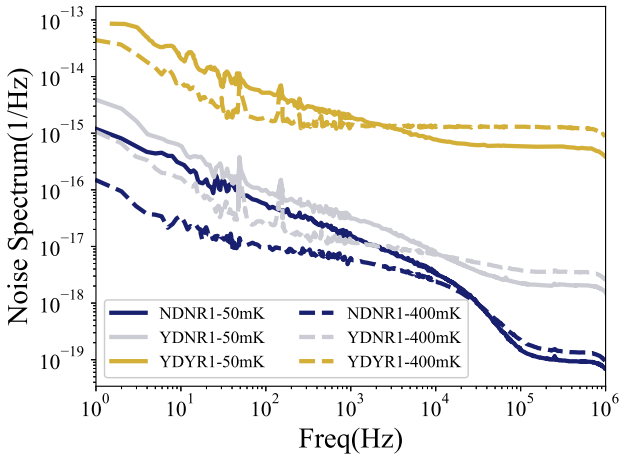

Figure 3: Normalized frequency noise sampled at 10 MHz of one pixel in each of the three samples of the first design measured at two different bath temperatures (50 mK for continuous lines and 400 mK for dashed lines) and a fixed input power of -100 dBm.

$$M_{\text{tot}} = \begin{bmatrix} M_{11} & M_{12} \\ M_{21} & M_{22} \end{bmatrix} = \prod_{p=1}^{P} M_p$$
$$= \prod_{p=1}^{P} \begin{bmatrix} \cos(\tilde{k}_p d_p) & j\eta_p \sin(\tilde{k}_p d_p) \\ j\eta_p^{-1} \sin(\tilde{k}_p d_p) & \cos(\tilde{k}_p d_p) \end{bmatrix} \quad (1)$$

where d_p is the length of the transmission line p, corresponding to the thickness of the thin-film. The modelled total reflection R_m and transmission T_m through the optical stack can then be extracted from Eq. 1 as $R_m = |M_{11}|^2$ and $T_m = |M_{12}|^2$.

In our previous paper[9], we demonstrated by spectrometry that a non-negligible part of incident photons is transmitted through the TiN absorber and that adding a transparent Al_2O_3 dielectric layer underneath would not affect transmittance. We have generalized this concept in Fig. 2 for multiple dielectric thicknesses and observe a clear dependence between reflectance and photon wavelength. Since Al and Al_2O_3 have respectively near-unity reflectance and transmittance in the 400-1600 nm range, most of the incident photons transmitted through the TiN layer are trapped inside what we could describe as a cavity, resulting in most of them being eventually absorbed by the TiN inductor. If we assume that the number of incident photons reflected on the fixed 30 nm TiN thickness is independent of the variable dielectric thickness underneath, then, the reflectance variation in Fig 2 represents the optical stack photon coupling to the absorber. Thus, the minimum reflectance corresponds to the most photons trapped inside the cavity and is reached at the guided quarter-wavelength distance between the reflector and inductor $\lambda/4n$, a characteristic distance commonly used for detectors coupled to a backshort cavity. As a result, for our laser diode emitting at $\lambda = 405$ nm, the dielectric thickness must be $405/(4 \times 1.7) \approx 60$ nm.

3. Noise analysis of each optical stack layer

To quantify the noise influence of each layer composing the optical stack, we have fabricated three different samples of 25-pixel arrays introduced previously as NDNR1, YDNR1 and YDYR1 with resonances in the 2-3.5 GHz range. The samples are read out using the standard homodyne detection scheme[2, 14, 15] and cooled down in an Adiabatic Demagnetization Refrigerator (ADR) at bath temperatures ranging from 400 mK ($T_c/10$) down to 50 mK ($T_c/20$) with a maximum input power of -100 dBm without saturating. The starting frequency is around 2 GHz in all three samples, so the optical stack parasitic capacitance of YDYR1 computed in our last paper[9] has little influence over the resonance frequency as expected. However, there is a significant contrast of quality factors between samples as reported in Table 1. We can analyze the frequency noise of all three samples by plotting the Power Spectral Density (PSD) normalized by the total quality factor:

$$PSD_{1/\text{Hz}} = \frac{PSD_{\text{rad}^2/\text{Hz}}}{(4Q)^2} \quad (2)$$

to maintain similar slopes between samples regardless of Q. The PSD of all 3 samples is plotted in log-log scale in Fig. 3.

Table 1: Measured parameters of one MKID in every sample discussed in this study designated by their acronyms and in parenthesis the thin-films constituting the optical stack with the absorbing part of the resonator being either TiN ($T_c \approx 4$ K) or TiN/Ti/TiN ($T_c \approx 1.3$ K). All values reported in this table are measured at a bath temperature of 50 mK and maximum input power before saturation noted as $P_r^{\max}$. Since no photon-counting was achieved at 50 mK because of TLS noise, the energy-resolving power values are all measured around their respective MKID usual operating temperatures $\sim T_c/10$.

	$P_r^{\max}$ (dBm)	f_r (GHz)	Q_i	PSD @1kHz (Hz^{-1})
NDNR1 (single-layer TiN)	-100	3.43	3×10^5	2×10^{-17}
YDNR1 (single-layer TiN/Al_2O_3)	-100	3.42	5×10^4	4×10^{-17}
YDYR1 (single-layer TiN/Al_2O_3/Al/Nb)	-100	3.12	1×10^4	2×10^{-15}
NDNR2 (single-layer TiN)	-90	2.01	5×10^4	1×10^{-17}
YDYR2 (single-layer TiN/Al_2O_3/Al/Nb)	-90	2.55	2.5×10^4	5×10^{-16}
NDNR2 (tri-layer TiN/Ti/TiN)	-85	3.12	3×10^3	1×10^{-18}
YDYR2 (tri-layer TiN/Ti/TiN/Al_2O_3/Al/Nb)	-85	2.82	2×10^3	7×10^{-16}

For frequencies lower than 20 Hz, the noise spectrum is dominated by f^{-1} noise regardless of bath temperature. This is primarily attributed to the IQ mixer and amplifiers used in the system. Between 20 Hz and 10 kHz, the signature of TLS noise is present but only at 50 mK, showing a clear $f^{-1/2}$ dependence. Above the resonators roll-off frequency starting at ~10 kHz, the PSDs reach the noise floor given by the readout noise and scales with bath temperature. The noise spectrum at 10^3 Hz taken from Fig. 3 reported in Table 1 shows that the addition of a dielectric layer below the absorber has doubled the frequency noise from 2×10^{-17} Hz^{-1} in NDNR1 to 4×10^{-17} Hz^{-1} in YDNR1. This relatively slight noise increase in YDNR1 is certainly explained by the amorphous Al_2O_3 layer being lossy. However, for the full optical stack sample YDYR1, we measure a much larger noise amplification of two orders of magnitude compared to the reference sample for any frequency below the resonator roll-off frequency. The minute parasitic capacitance between the reflector and superconductor is suspected to host non-saturated TLS responsible for this increase. This makes determining the energy of incoming photons unrealistic, unless the gain in signal due to the presence of the reflector is large enough to surpass the relative noise increase. At 400 mK, the only visible noise signatures in the optical stack sample PSD (dashed yellow line) are f^{-1} noise and readout noise. This is because the Q_i is so low at 50 mK that when we increase bath temperature, the resonance dip disappears completely before reaching 400 mK. Since the optical stack sample has such a low Q_i, we have fabricated a second batch described in the introduction for which the major difference is the use of a higher-T_c material (Nb) for the IDC to help decrease loss. At 50 mK, the Q_i of YDYR2 reported in Table 1 has more than doubled compared to YDYR1.

In the previous paper[9], we have presented graphically the influence of the optical stack over the resonator by plotting the fractional frequency shift $\Delta f/f$ as a function of temperature. The signature of TLS in the optical stack sample was highlighted by the resonator shift towards higher frequencies below the TLS turning point at 250 mK, widely reported in the literature. As expected for this updated design whose absorber is still a stoichiometric TiN inductor, the same behavior has been observed.

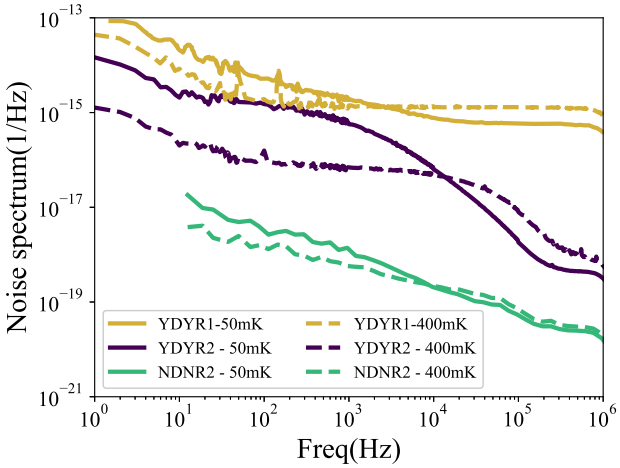

Figure 4: Normalized frequency noise sampled at 10 MHz of one pixel in each of the two samples of the second design with a single-layer TiN absorber measured at two different bath temperatures (50 mK for continuous lines and 400 mK for dashed lines) and a fixed input power of -90 dBm. The PSD of YDYR1 from Fig. 3 is plotted again for comparison. The noise below 10 Hz for NDNR2 was not measured.

In Fig. 4, we have plotted the PSDs of the two samples of this second design and added the optical stack sample of the first design for comparison.

Since there are no major difference at low and high frequencies compared to Fig. 3, we will only focus on the 10 Hz to 10 kHz range. In this range, NDNR2 has the lowest noise level as one would expect, regardless of temperature. At 1 kHz, the noise at the usual MKID operating temperature ($T_c/10 \approx 400$ mK) shown as a green dashed line for NDNR2 is around 4×10^{-18} Hz^{-1} which is the lowest we have obtained so far. However, for the optical stack sample YDYR2, the measured PSD at the same temperature and frequency is 6×10^{-17} Hz^{-1}, which is more than one order of magnitude higher than the reference sample. All the parameters measured for these samples at 50 mK can be found in Table 1. Another interesting observation lies in the slope of the PSDs. The reference sample has a slightly steeper noise slope at 50 mK compared to 400 mK, showing a small increase in TLS noise at lower temperatures. However, for the optical stack sample YDYR2 at 400 mK (dashed purple line), there is almost no difference in slope between 10 Hz and 1 kHz which lays almost flat, indicative of white noise free of TLS. For comparison, the noise slope of the same resonator at 50 mK (purple continuous line) is proportional to $f^{-1/2}$, characteristic of TLS noise present in the vicinity of the resonator [16, 12] which is also noticeable for the previously measured YDYR1 at the same bath temperature (yellow continuous line). This increase in TLS is consistent with the inverse phase response observed for sample YDYR2 in the next section when illuminating it with optical pulses at 50 mK. Since the only difference between the samples is the addition of the optical stack, we believe its influence over the resonator is substantial. The increase in TLS noise might originate from the two additional interfaces in the optical stack that have suffered uncontrolled oxidation between deposition, leading to amorphous layers prone to host TLS. Indeed, during the reference sample fabrication process, the TiN meander (the most critical part of the resonator) is deposited directly on the single-crystal sapphire substrate right after acid cleaning. For the optical stack sample, the meander is deposited on top of the Al_2O_3 dielectric layer that might be partially amorphous and on which we do not control the surface contamination. Beyond the fabrication challenges, the optical stack and the meander form a Parallel-Plate Capacitor (PPC) described in the previous paper where a weak, non-saturating electric field also prone to TLS might reside. For the same capacitance value, the frequency noise of PPC is higher than for IDCs [17] and scales inversely proportional to their surface in the same fashion as for IDCs [18].

4. Optical illumination response

We have characterized the optical response of the samples using a commercial optical fiber SM980-5.8-125 and a 405 nm laser diode controlled by a pulse generator. The fiber is set at a distance of 35 mm to the sample that receives a light cone of 5 mm in diameter which is large enough to illuminate all 25 pixels. The entire optical illumination and homodyne measurement setup has already been described in great detail previously [15]. The phase response in the time domain of NDNR2 and YDYR2 are presented in Fig. 5 at the same two temperatures used for the noise analysis in the previous section: one above the TLS turning point ($\sim$ 250 mK for stoichiometric TiN) and one below. At 50 mK, a large and noisy inverse phase response is observed for YDYR2 whose relaxation time is 100 times longer than the normal phase response at 400 mK. This phenomenon has been attributed to a thermal perturbation in the resonator following the recombination of quasiparticles within the meander [19]. The generated phonons then interact with the non-saturated TLS abundant at temperatures $\leq T_c/10$ in the dielectric bulk and amorphous layers, resulting in a rapid change of dielectric constant that generates a transient phase shift in the resonator through the capacitor. This inverse phase response scales with decreasing temperature and decreasing input power. For NDNR2 (green lines), we observe a smooth and conventional phase response from Cooper pair breaking but no inverse response, indicating a much weaker TLS. We have obtained a single-photon response with NDNR2 measured at -85 dBm for multiple bath temperatures ranging from 200 mK to 700 mK. The maximum energy-resolving power $R = E/\Delta E$ reported in Table 2 has an optimum of 1.0 around 400 mK which corresponds to a bath temperature high enough to saturate TLS but low enough to have a high Cooper pair density [20]. As for YDYR2, at 400 mK when the TLS is saturated (dashed purple line), the inverse response disappears, giving way to a conventional but noisy phase shift ~ 1.5 times larger than for the reference sample. However, despite this improved response, no single-photon mode was observed.

We have also investigated whether adding superconducting layers so close to the absorber would unwantedly change its properties through the proximity effect. Since the coherence length of Al is largely superior to the spacer layer thickness, we suspect that it could affect the intrinsic properties of the TiN absorber and be responsible for the increased noise. One indirect method to verify this hypothesis is to compare the quasiparticle lifetime of the optical stack sample relative to the reference sample in Fig 6. Despite the relatively poor fitting of the YDYR2 tri-layer noisy

Table 2: Maximum energy-resolving power $R^{\max}$ of each sample in this study at the corresponding temperature $T^{\max}$. The input power used is the maximum input power before saturation $P_r^{\max}$ already presented in Table 1. The response to short optical pulses (405 nm) has been recorded for every sample between 50 and 700 mK and only three samples have reached single-photon mode. Out of these three, only the YDYR2 tri-layer has the optical stack.

	$T^{\max}$ (mK)	$R^{\max}$
NDNR1	–	–
YDNR1	–	–
YDYR1	–	–
NDNR2 single-layer	400 mK	1.0
YDYR2 single-layer	–	–
NDNR2 tri-layer	225 mK	3.2
YDYR2 tri-layer	225 mK	1.3

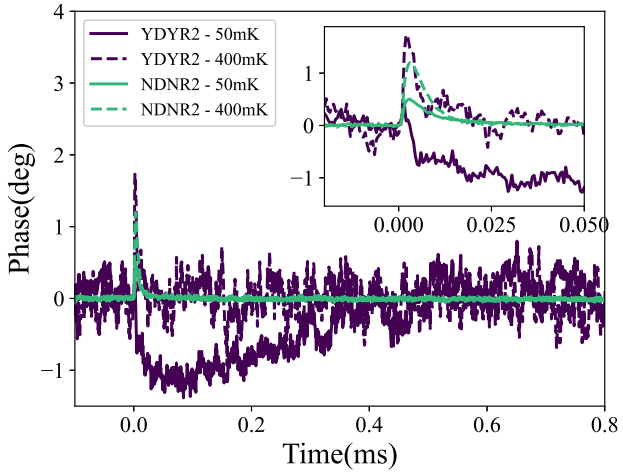

Figure 5: Averaged phase response in the time-domain of the resonators with and without the optical stack. Both samples were illuminated by a 405 nm diode with pulse widths of 50 ns and optical power of 4 pW. The response is represented at two different temperatures 50 and 400 mK and the attenuation on the readout path is -100 dBm.

phase response, both samples follow a temperature-dependent exponential decay as expected from known models [21] with a similar electron-phonon scattering time that suggests no major influence from the reflector on the absorber.

Since we were not able to reach single-photon counting with the single-layer stoichiometric TiN absorber embedded in the optical stack, we have fabricated an additional sample with a TiN/Ti/TiN tri-layer while keeping the same optical stack geometry of YDYR2 already presented in Fig. 1a. A TiN/Ti

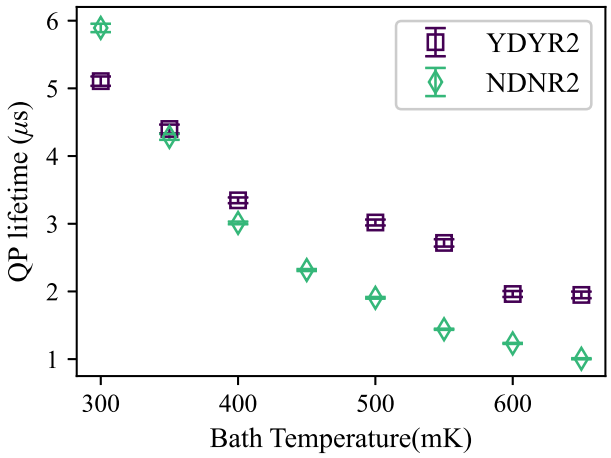

Figure 6: Quasiparticle relaxation time of both samples as a function of bath temperature. The larger uncertainty over the purple dots (YDYR2) is caused by the sample's higher noise level, illustrated in Fig. 5, making it hard to fit and extract an accurate relaxation time properly.

multi-layer acts as a single-layer thanks to the proximity effect with a T_c that can be tuned depending on the proportion of TiN thickness to Ti. This allows better sensitivity than a single-layer of TiN by reducing T_c of the absorber while achieving similar quality factors but better uniformity and homogeneity than sub-stoichiometric TiN_x [22, 23]. In such a multi-layer structure, increasing the thickness of the pure Ti layer over the TiN layers decreases the T_c but increases loss. To obtain a $T_c \approx 1$ K, we have found that the optimal ratio for the TiN/Ti/TiN tri-layer is 1:3:1. Since it is difficult in our sputtering system to accurately control the thickness of layers below 10 nm, the minimum total thickness layer of the multilayer would be achieved if both outer TiN layers are 10 nm-thick, and the inner pure Ti layer is 30 nm-thick. The optical parameters of this tri-layer will naturally be slightly different from the single-layer, but we assume that the optical stack optimization of the dielectric thickness covered in Sec. 2 is not related to this change. After fabrication, the corresponding film parameters are measured at a critical temperature $T_c = 1.29$ K with a resistivity before the superconducting transition $\rho_n = 80.2$ μΩ·cm. This new batch has been fabricated in the same fashion as batches discussed previously and consists of the reference sample NDNR2 tri-layer and the optical stack sample YDYR2 tri-layer with very similar quality factors, respectively 3×10^3 and 2×10^3 at usual operating temperatures ($\sim T_c/10$). The samples are illuminated with short pulses in the same conditions as previous samples. The phase response is processed with an optimal

filter commonly used for MKIDs to account for their frequency-dependent noise [4, 10]. The statistics of the resonator's response for NDNR2 tri-layer and YDYR2 tri-layer are respectively represented in Fig. 7a and Fig. 7b. While the single-photon response is observed for the optical stack sample, the maximum energy-resolving power measured at $\sim$ 225 mK and -85 dBm is almost three times lower than for the reference sample at the same bath temperature and input power. This is probably related to the additional noise sources mentioned previously in the optical stack. In the current state, it is thus irrelevant to determine the gained quantum efficiency from the optical stack as it degrades the energy-resolving power. Since most of this additional noise comes from the dielectric, we are currently investigating the possibility of suspending the absorber above the reflector with only a vacuum in between. Granting that this method would complicate an already tedious fabrication process, we have previously demonstrated the feasibility of suspending a superconducting thin-film used as the upper electrode of a MIM capacitor [17]. This new YDYR3 design would have the edges of the absorber rest directly onto the substrate to create anchor points, while the rest of the absorber would be suspended above a previously deposited reflecting layer.

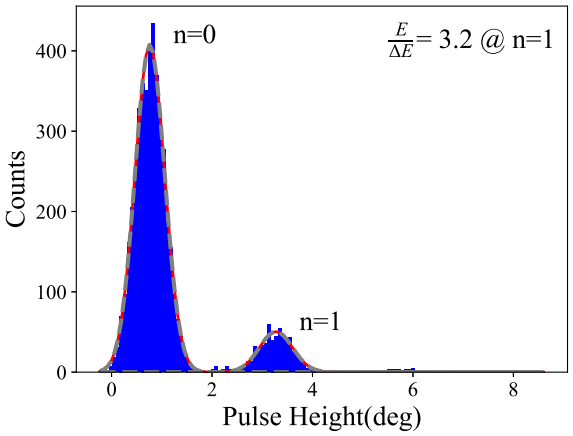

(a) NDNR2 tri-layer

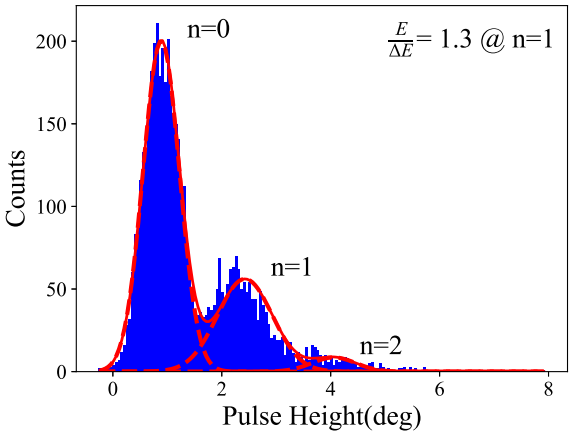

(b) YDYR2 tri-layer

Figure 7: Resonators phase response to short pulse illuminations fitted as a Poisson distribution for (a) the reference and (b) optical stack samples with the meander patterned as a TiN/Ti/TiN tri-layer. The maximum energy-resolving power shown at n = 1 photon event was recorded around 225 mK and -85 dBm for both samples.

5. Conclusion

We have investigated the noise and optical response of MKIDs with an optical stack geometry that consists of a Nb/Al reflector and an Al_2O_3 dielectric layer with a thickness optimized for $\lambda = 405$ nm.

We fabricated three samples (full, partial and no optical stack) with fully stoichiometric TiN LC resonators to independently evaluate the noise of each layer forming the optical stack. We notice that the addition of the dielectric layer below the inductive absorber without the reflector did not significantly affect the resonator's Q_i nor its noise level. However, the Q_i of the full optical stack suffered greatly with an increase of noise by a factor of 100, showing that the full optical stack must act as a parasitic capacitor that deteriorates the MKIDs performance.

In order to better characterize the noise and optical response of the full optical stack, we fabricated a full optical stack sample and a reference sample, where the IDC and its inductive arms are patterned with a higher T_c material (Nb). It allowed to control the absorber's thickness independently from the IDC and also, to avoid parasitic photon detection and loss coming from the inductive arms of the IDC. Despite having higher Q_i factors, the PSD of the full optical stack still shows a clear noise increase at lower temperatures and a slope of -1/2, characteristic of TLS noise. Unfortunately, photon counting was only obtained for the reference sample but not for the optical stack sample.

We finally obtained photon counting with the optical stack by replacing the single-layer TiN film by a tri-layer TiN/Ti/TiN film with a lower T_c. However, the energy-resolving power of the tri-layer full optical stack sample is degraded compared to the tri-layer reference sample. This is probably due to the additional TLS noise in the Al_2O_3 dielectric and at the absorber/dielectric and dielectric/reflector interfaces. For these reasons, we believe that one of the most viable solutions in this configuration would be to suspend the meander above the reflector to replace Al_2O_3 by vacuum. This would significantly reduce TLS

noise at the cost of a more complex fabrication process that would nevertheless be achievable.

Data availability statement

The data that support the findings of this study are available upon request from the authors.

Acknowledgments

The authors would like to thank Dr. Michael Rosticher at ENS for the deposition of Al_2O_3 by ALD, Florent Reix at GEPI for wafer cutting, and the AstroParticules et Cosmologie laboratory for kindly allowing measurements in their ADR cryostat. The authors also thank Dr. Boon Kok-Tan at Oxford university for helpful discussion. This work was supported by the European Research Council through grant 835087 (SPIAKID) and by the French space agency Centre National d'Etudes Spatiales (CNES).

References

[1] Meeker S R, Mazin B A, Walter A B, Strader P, Fruitwala N, Bockstiegel C, Szypryt P, Ulbricht G, Coiffard G, Bumble B, Cancelo G, Zmuda T, Treptow K, Wilcer N, Collura G, Dodkins R, Lipartito I, Zobrist N, Bottom M, Shelton J C, Mawet D, Van Eyken J C, Vasisht G and Serabyn E 2018 PASP **130** 65001 URL https://doi.org/10.1088/1538-3873/aab5e7

[2] Beldi S, Boussaha F, Hu J, Monfardini A, Traini A, Levy-Bertrand F, Chaumont C, Gonzales M, Firminy J, Reix F, Rosticher M, Mignot S, Piat M and Bonifacio P 2019 Opt. Express **27** 13319–13328 URL https://doi.org/10.1364/oe.27.013319

[3] Walter A B, Fruitwala N, Steiger S, Bailey J I, Zobrist N, Swimmer N, Lipartito I, Smith J P, Meeker S R, Bockstiegel C, Coiffard G, Dodkins R, Szypryt P, Davis K K, Daal M, Bumble B, Collura G, Guyon O, Lozi J, Vievard S, Jovanovic N, Martinache F, Currie T and Mazin B A 2020 PASP **132** 125005 URL https://doi.org/10.1088/1538-3873/abc60f

[4] de Visser P J, de Rooij S A, Murugesan V, Thoen D J and Baselmans J J 2021 Phys. Rev. Applied **16** 034051 URL https://doi.org/10.1103/PhysRevApplied.16.034051

[5] Szypryt P, Mazin B A, Ulbricht G, Bumble B, Meeker S R, Bockstiegel C and Walter A B 2016 Appl. Phys. Lett. **109** 151102 URL https://doi.org/10.1063/1.4964665

[6] Dai M, Guo W, Liu X, Zhang M, Wang Y, Wei L F, Hilton G C, Hubmayr J, Ullom J, Gao J and Vissers M R 2019 J. Low Temp. Phys. **194** 361–369 URL https://doi.org/10.1007/s10909-018-2095-9

[7] Kouwenhoven K, Elwakil I, van Wingerden J, Murugesan V, Thoen D J, Baselmans J J A and de Visser P J 2021 J. Low Temp. Phys. **209** 1249–1257 URL https://doi.org/10.1007/s10909-022-02774-0

[8] Mai Z, Dai X, Chen Y, Shi Z, Wang H, Pan C, Liu X, Wang Z, Guo W and Wang Y 2023 Appl. Opt. **62** 5294–5300 URL https://doi.org/10.1364/AO.493305

[9] Nicaise P, Hu J, Martin J M, Beldi S, Chaumont C, Bonifacio P, Piat M, Geoffray H and Boussaha F 2022 J. Low Temp. Phys. **209** 1242–1248 URL https://doi.org/10.1007/s10909-022-02789-7

[10] Mazin B A, Meeker S R, Strader M J, Szypryt P, Marsden D, van Eyken J C, Duggan G E, Walter A B, Ulbricht G, Johnson M, Bumble B, O'Brien K and Stoughton C 2013 PASP **125** 1348 URL https://doi.org/10.1086/674013

[11] Swimmer N, Mazin B A, Bockstiegel C, III J I B, Coiffard G, Daal M, Davis K, Fruitwala N, Lipartito I, Smith J, Steiger S, Zobrist N, Cook T, Chakrabarti S, Mendillo C, Martel J and Hewawasam K 2020 **11447** 114479B URL https://doi.org/10.1117/12.2561770

[12] Guo W, Liu X, Wang Y, Wei Q, Wei L F, Hubmayr J, Fowler J, Ullom J, Vale L, Vissers M R and Gao J 2017 Appl. Phys. Lett. **110** 212601 URL https://doi.org/10.1063/1.4984134

[13] Nestell J E and Christy R W 1972 Appl. Opt. **11** 643–651

[14] Hu J, Salatino M, Traini A, Chaumont C, Boussaha F, Goupil C and Piat M 2020 J. Low Temp. Phys. **199** 355–361 URL https://doi.org/10.1007/s10909-019-02313-4

[15] Hu J, Nicaise P, Boussaha F, Martin J M, Chaumont C, Marret A, Reix F, Firminy J, Vacelet T, Pham V D et al. 2023 J. Low Temp. Phys. URL https://doi.org/10.1007/s10909-023-03018-5

[16] Gao J, Daal M, Martinis J M, Vayonakis A, Zmuidzinas J, Sadoulet B, Mazin B A, Day P K and Leduc H G 2008 Appl. Phys. Lett. **92** 212504 URL https://doi.org/10.1063/1.2937855

[17] Boussaha F, Beldi S, Monfardini A, Hu J, Calvo M, Chaumont C, Levy-Bertrand F, Vacelet T, Traini A, Firminy J, Piat M and Reix F 2020 J. Low Temp. Phys. **199** 994–1003 URL https://doi.org/10.1007/s10909-019-02309-0

[18] Doyle S, Mauskopf P, Naylon J, Porch A and Duncombe C 2008 J. Low Temp. Phys. **151** 530–536 URL https://doi.org/10.1007/s10909-007-9685-2

[19] Hu J, Boussaha F, Martin J M, Nicaise P, Chaumont C, Beldi S, Piat M and Bonifacio P 2021 Appl. Phys. Lett. **119** 212601 URL https://doi.org/10.1063/5.0074103

[20] Boussaha F, Hu J, Nicaise P, Martin J M, Chaumont C, Dung P V, Firminy J, Reix F, Bonifacio P, Piat M and Geoffray H 2023 Appl. Phys. Lett. **122** 212602 URL https://doi.org/10.1063/5.0147584

[21] Barends R, Baselmans J J A, Yates S J C, Gao J R, Hovenier J N and Klapwijk T M 2008 Phys. Rev. Lett. **100** 257002 URL https://doi.org/10.1103/PhysRevLett.100.257002

[22] Faverzani M, Ferri E, Giachero A, Giordano C, Margesin B, Mezzena R, Nucciotti A and Puiu A 2020 Supercond. Sci. Technol. **33** 045009 URL https://doi.org/10.1088/1361-6668/ab7435

[23] Lucia M D, Baldwin E, Ulbricht G, Piercy J D, Creaner O, Bracken C and Ray T P 2022 **12191** 1219105 URL https://doi.org/10.1117/12.2626867